JOURNAL OF GEOPHYSICAL RESEARCH, VOL. 106, NO. A12, PAGES 29,515–29,529, DECEMBER 1, 2001

Stochastic growth of waves over Earth's polar cap

Iver H. Cairns
School of Physics, University of Sydney, Sydney, New South Wales, Australia.

J. D. Menietti
Department of Physics and Astronomy, University of Iowa, Iowa City, Iowa, USA

Abstract. Bursty waves with widely varying electric fields persist over a wide range of altitudes $\sim 2-7\ R_E$ at polar cap latitudes in Earth's inner magnetosphere. These "PF" waves have frequencies near expected values of the electron plasma frequency (PF), well below the electron gyrofrequency, and are believed to be generated by electron beams. Here it is demonstrated that stochastic growth theory (SGT) can account well for the detailed field statistics of the archetypal PF wave event, by showing that the observed distributions $P(\log E)$ of envelope electric fields E are well fitted by the lognormal function predicted by SGT. Weak evidence exists that a nonlinear wave process coexists with stochastic growth physics at large fields $\gtrsim 1$ mV m^{-1} on the basis of fits of the observed $P(\log E)$ distribution to the SGT prediction that includes a nonlinear process at high fields and on the discovery of a class of low-frequency waves that may be produced by nonlinear decay of PF waves. An analytic model is developed for why the waves evolve to an SGT state, on the basis of waves driven by an electron beam in MHD density turbulence and the development of fluctuations in the electron beam due to wave growth occurring in localized regions. The model is viable for the polar cap plasma parameters considered, predicting that the wave burstiness should be of order that observed and that the beam fluctuations should have timescales ~ 10 ms that are below current detection capabilities. SGT thus accounts well for the burstiness and wave statistics, as well as the persistence of the waves and driving distribution. The consistency of the PF wave statistics with SGT also implies the presence of local electron beams over much of the polar cap, whose source is currently unknown. This application brings to five the number of contexts in which SGT applies, suggesting that SGT is widely applicable in space plasmas.

1. Introduction

"Plasma frequency" or PF waves are bursty electromagnetic waves observed over Earth's polar caps and auroral zones [*Cairns and Menietti,* 1997; *Menietti et al.,* 1998]. The waves are relatively narrowband with frequencies that are typically a factor of $\sim 2-4$ below the measured electron gyrofrequency f_g but comparable to the electron plasma frequency f_p estimated from wave data or measured directly at these altitudes [*Gurnett et al.,* 1983; *Persoon et al.,* 1983, 1988; *Cairns and Menietti,* 1997; *Menietti et al.,* 1998]. The waves are observed by Dynamics Explorer 1 (DE-1) at all magnetic longitudes, with a concentration on the nightside, and at radial distances from 2 to 4.5 Earth radii R_E [*Menietti et al.,* 1998]. These data imply that the waves and associated driving particle distributions extend and persist over distances $\gtrsim 2\ R_E$. Polar data show PF-like waves out to radial distances of order 8 R_E (J. D. Dorelli et al., unpublished manuscript, 2000), suggesting persistence of the waves and driving distributions for $\sim 6\ R_E$. Emissions at twice the frequency of the PF band are also observed by DE 1, the so-called harmonic or "H component", and interpreted in terms of z mode waves near $2f_p$ [*Cairns and Menietti,* 1997; *Menietti et al.,* 1998]. PF waves are typically much more bursty, intense, and narrowband than whistler mode hiss, which is widely believed to be generated at low heights along auroral field lines [*Gurnett et al.,* 1983]. Propagation of hiss to higher latitudes naturally results in a funnel shape in dynamic spectra [*Gurnett et al.,* 1983], with a high-frequency cutoff at f_p predicted by cold plasma theory when $f_p \leq f_g$ [*Gurnett et al.,* 1983; *Persoon et al.,* 1983, 1988].

The burstiness and widely variable fields of PF waves imply local generation of the waves, perhaps by either

Paper number 2000JA000422.
0148-0227/01/2000JA000422$09.00

an electron beam or temperature anisotropy instability [*Cairns and Menietti,* 1997; *Menietti et al.,* 1998; *Gary and Cairns,* 1999; *Gary et al.,* 2000]. On the basis of the observed frequencies and differences from auroral hiss, *Cairns and Menietti* [1997] favored interpreting PF waves as z mode emissions, perhaps in superposition with whistler mode waves. Investigation of the wave polarization [*Menietti et al.,* 1998] reveals that 22% of the 113 periods analyzed had left-hand polarization, thereby being directly consistent with the z mode (at frequencies below f_p) but inconsistent with the whistler mode, while 9% of the events had right-hand polarization and so were consistent with either the whistler mode or with the z mode for frequencies above f_p. The remaining 69% of events had indeterminate polarization, perhaps due to superposition of z and whistler waves [*Menietti et al.,* 1998] or due to the waves being primarily electrostatic with weak circular polarization [*Gary et al.,* 2000].

Recent linear theory analyses reveal that it is very difficult to drive z mode waves directly with a perpendicular/parallel electron temperature anisotropy [*Gary and Cairns,* 1999] or, when $f_p < f_g$, with a nonrelativistic electron beam [*Gary et al.,* 2000; *Willes and Cairns,* 2000]. In a magnetized kinetic plasma with $f_p < f_g$ the Langmuir and whistler modes combine [*Melrose,* 1980; *Willes and Cairns,* 2000] into a generalized Langmuir mode with Langmuir-like dispersion above f_p (where the whistler mode has a high-frequency resonance in cold plasma theory) and whistler-like dispersion below f_p (where the Langmuir has a cutoff according to unmagnetized theory), while the z mode remains essentially as predicted by cold plasma theory in this regime. The Langmuir/whistler mode has a right-hand sense of polarization at all wave numbers k and is driven unstable by plausible electron beams [*Gary et al.,* 2000; *Willes and Cairns,* 2000]. Another possibility is that sufficiently dense electron beams drive the beam mode unstable; this mode has $\omega \approx kv_b$ for beam speed v_b, is not a normal mode of the background plasma, and is usually primarily electrostatic but with a right-hand sense of polarization [*Gary et al.,* 2000; *Willes and Cairns,* 2000]. In contrast, for $f_p < f_g$, z mode waves with frequencies $\sim f_p$ have wave numbers $kc \lesssim 2\pi f_p$ that are not resonantly excited by nonrelativistic electron beams and have left-hand polarization.

At present, the most likely scenario involves electron beams driving the PF waves as either beam mode or Langmuir/whistler waves with right-hand polarization and that left-hand polarization develops because of conversion into the z mode by nonlinear or other processes [*Gary and Cairns,* 1999; *Gary et al.,* 2000; *Willes and Cairns,* 2000]. Observations by Polar show nonthermal streaming electrons with beam and loss cone anisotropies over the polar cap during times when PF-like waves are present (J. D. Dorelli et al., unpublished manuscript, 2000). These electron beams evidently persist far from their likely source regions over the polar cap or auroral zone.

The primary goal of this paper is to demonstrate that stochastic growth theory (SGT) can account for the functional form of the field statistics of PF waves and so for the waves' burstiness, widely varying fields, and persistence. SGT is a general theory that provides a natural, quantitatively testable explanation for bursty, persistent waves and their driving distributions [*Robinson,* 1992, 1995; *Robinson et al.,* 1993a; *Cairns and Robinson,* 1997, 1999; *Cairns et al.,* 2000], including situations where thermal waves or nonlinear processes are relevant. Section 2 gives a brief introduction to SGT. As described there, the primary means of testing SGT is to compare the observed probability distribution $P(\log E)$ of envelope electric fields E with the theoretical predictions; in the case of pure SGT the $P(\log E)$ distribution is Gaussian in $\log E$. SGT is quantitatively consistent with Langmuir/z mode waves observed in interplanetary type III solar radio burst sources [*Robinson et al.,* 1993a], Langmuir/z mode waves observed relatively deep in Earth's foreshock [*Cairns and Robinson,* 1997, 1999], thermal Langmuir/z waves in the solar wind [*Cairns et al.,* 2000], and driven thermal waves near the edge of Earth's foreshock [*Cairns et al.,* 2000].

The present paper represents the first application of SGT to waves other than the Langmuir/z mode waves studied in the above solar wind and foreshock analyses; in this case, as discussed above, the waves are instead z mode, beam mode, or Langmuir/whistler waves, either separately or together. One corollary of this successful application of SGT is that the waves are necessarily being driven locally. A second corollary is that SGT demonstrably applies now to five different wave phenomena in space, thereby being increasingly well described as "widely applicable".

The secondary goal of this paper is to infer the occurrence of a nonlinear process for the PF waves, using modifications at high E to the $P(\log E)$ distribution predicted by pure SGT. A secondary line of evidence for this nonlinear process is the existence and properties of low-frequency waves that are correlated with bursts of PF waves and are interpreted as daughter waves resulting from nonlinear decay of PF waves.

The paper is structured as follows. Section 2 introduces SGT and the corresponding theoretical predictions for the distribution $P(\log E)$. The wave data and characteristics of the source plasma are summarized in section 3. The statistics of PF fields are demonstrated in section 4 to have the functional form predicted by SGT, with weak evidence for a nonlinear process operating at high wave fields. In section 5 a new class of low-frequency waves is identified in the wave data and then interpreted in terms of this nonlinear process. Section 6 contains an analytic model for why PF waves attain an SGT state. These results are discussed in section 7 and the conclusions are given in section 8.

2. Review of Stochastic Growth Theory

SGT is an attractive theory for explaining bursty waves with widely varying fields that persist with the associated driving particle distributions far from their source [*Robinson*, 1992, 1995; *Robinson et al.*, 1993a,b; *Cairns and Robinson*, 1997, 1999; *Cairns et al.*, 2000]. Plasma theory has long recognized the tendency for wave-particle interactions to drive a system toward marginal stability [*Stix*, 1962, 1992; *Krall and Trivelpiece*, 1973; *Melrose*, 1980, 1986], where wave emission and damping are balanced. SGT treats situations in which a driving particle distribution interacts self-consistently with its driven waves in an inhomogeneous plasma and evolves to a state in which (1) the particle distribution is close to time- and volume-averaged marginal stability but with stochastic fluctuations that (2) cause the wave gain G to vary stochastically in time and space. The gain $G(t)$ at time t is defined by

$$G = \int_{-\infty}^{t} dt' \, \Gamma(t') \tag{1}$$

and is related logarithmically to the envelope electric field $E(t)$ by

$$G = \ln(E(t)/E_0) \, , \tag{2}$$

where $\Gamma(t')$ is the linear growth rate at time t' and E_0 is a reference field.

The hypothesized random walk in G and the logarithmic relation between $E(t)$ and $G(t)$ provide an immediate and natural qualitative explanation for the burstiness and widely varying nature of the wave fields. Similarly, the closeness to marginal stability provides an immediate qualitative explanation for the persistence of the waves and unstable particle distribution far from the source of the unstable distribution. In contrast, the "uniform secular" model for wave growth in plasmas [e.g., *Stix*, 1962, 1992; *Krall and Trivelpiece*, 1973; *Melrose*, 1980, 1986], of homogeneous exponential "linear" growth with constant growth rate until saturated by nonlinear processes, encounters major problems explaining the burstiness and widely varying fields of the waves and the persistence of the waves and driving distributions that are characteristic of space plasmas [*Robinson et al.*, 1993a; *Cairns and Robinson*, 1997, 1999].

SGT is formulated as a general theory, which can potentially apply to arbitrary combinations of wave mode, source of free energy, and inhomogeneous background plasma that satisfy hypotheses (1) and (2) above. The detailed route by which a given system evolves to an SGT state presumably depends upon the system. However, the qualitative physics is envisaged to be as follows: preexisting inhomogeneities in the plasma cause wave growth to be more effective in some regions than others, this wave growth induces spatiotemporal fluctuations in the driving particle distribution by quasi-linear relaxation, and the ensuing interactions of the fluctuating particle distribution and waves in the inhomogeneous background plasma lead to the waves and particles evolving to an SGT state. Next consider the relation $E(t) = E_0 \exp G(t)$ from (2) and rewrite the integral (1) as a sum $G(t) = \Sigma_i \Delta G_i = \Sigma_i \Gamma_i \Delta t_i$ over multiple successive fluctuations $\Delta G_i = \Gamma_i \Delta t_i$ of the wave gain, the growth rate, and the particle distribution function. Then, provided only that sufficiently many fluctuations in ΔG_i occur during some characteristic time, the Central Limit Theorem requires $G(t)$ to be a Gaussian random variable as assumed in hypothesis (2), irrespective of the detailed statistics of the fluctuations ΔG_i. Thus, since hypothesis (1) is justified by the tendency for all unstable wave-particle systems to approach marginal stability, the qualitative physical justifications for the SGT hypotheses are simple and natural. Accordingly, SGT has the potential to be widely applicable. An analytic model for why PF waves evolve to an SGT state is developed in section 6, on the basis of existing models in other systems [*Robinson et al.*, 1993a; *Cairns and Robinson*, 1997].

SGT is a statistical theory and hence the relevant theoretical quantities and associated observational and theoretical tests involve the statistics of the waves and driving particles. Examples are the probability distributions $P(G)$ and $P(\log E)$ of G and $\log E = \log_{10} E$, respectively. For pure SGT systems, in which thermal waves and nonlinear processes can be ignored, the Central Limit Theorem predicts that $P(G)$ and $P(\log E)$ should be Gaussian in G and $\log E$, respectively, [*Robinson*, 1992; *Robinson et al.*, 1993a; *Cairns and Robinson*, 1997, 1999]:

$$P(\log E) = (2\pi\sigma^2)^{-1/2} e^{(\log E - \mu)^2/2\sigma^2} \, , \tag{3}$$

where μ and σ are the average and standard deviation of $\log E$, respectively. This is the simplest, most fundamental test of SGT and is easily amenable to observational testing. Figure 1 shows this prediction using the solid line.

The dashed line in Figure 1 shows the corresponding analytic prediction for a situation in which a nonlinear process removes wave energy at high E above a threshold E_c and so decreases $P(\log E)$ below the prediction (3) [*Robinson et al.*, 1993a]:

$$\begin{aligned} P(\log E) &= \frac{1}{\sqrt{2\pi}\sigma A} \left[e^{-(\log E - \mu)^2/2\sigma^2} \right. \\ &- \left. e^{-(2\log E_c - \log E - \mu)^2/2\sigma^2} \right] \, , \end{aligned} \tag{4}$$

where the normalization factor

$$A = \mathrm{erf}\left(\frac{\log E_c - \mu}{\sigma\sqrt{2}} \right) \tag{5}$$

involves the conventional error function and preserves the normalization $\int d(\log E) P(\log E) = 1$ of the distri-

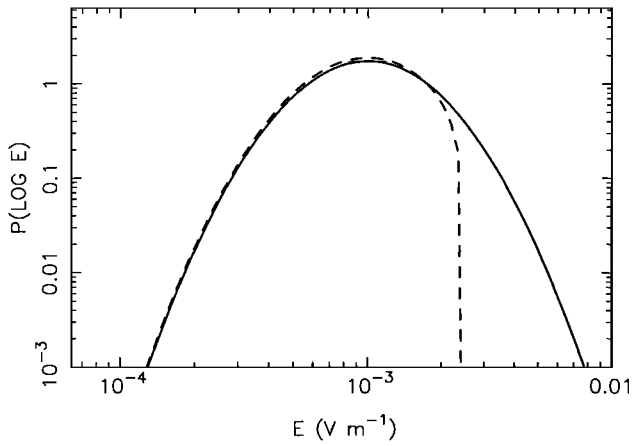

Figure 1. SGT predictions for the distribution $P(\log E)$ of wave fields for $\mu = -3.0$ and $\sigma = 0.23$. The solid line shows the prediction (3) for pure SGT, while the dashed line shows the prediction (4) for nonlinear SGT, in which a nonlinear process is active above a nonlinear threshold $E_c = 2.5$ mV m^{-1}.

bution. Note in both Figure 1 and (4) that the nonlinear process only decreases the $P(\log E)$ distribution below the prediction (3) at high $E \gtrsim E_c$; at lower $E \lesssim E_c$ the prediction (4) lies slightly above (3) due to the factor A^{-1}. Comparisons between the observed distribution $P(\log E)$ and the pure SGT prediction (3) and its counterpart (4) when a nonlinear process is active can thus be used to test the relevance of SGT and to determine also whether a nonlinear process is active at high E.

The uniform secular model for wave growth, of spatially homogeneous exponential amplification with a constant growth rate that continues until the wave field exceeds the lowest threshold for a nonlinear process and the growth is saturated [e.g., *Stix*, 1962, 1992; *Krall and Trivelpiece*, 1973; *Melrose*, 1980, 1986], predicts quite different $P(\log E)$ distributions from SGT. Suppose that the nonlinear process leads to exponential wave damping, as in nonlinear Landau damping (e.g., scattering off thermal ions) or a three-wave process which removes energy from the parent waves [e.g., *Stix*, 1962, 1992; *Krall and Trivelpiece*, 1973; *Melrose*, 1980, 1986]; i.e., the waves grow and damp exponentially, possibly with different (constant) growth or damping rates. If the field is sampled uniformly in time, then the $P(\log E)$ distribution for the exponential phases is uniform or flat (since each sample differs in $\log E$ by a constant amount) below and slightly above the nonlinear threshold but then has a rapid falloff at higher fields [*Robinson et al.*, 1993a]. A similar result holds for an ensemble of exponentially growing/damping waves sampled randomly in time: the $P(\log E)$ distribution is locally flat around each sample (since the growth/damping rate is constant) and sampling randomly in time means that each field sample is distributed randomly between the thermal level and the nonlinear threshold, so that the overall $P(\log E)$ distribution over many cycles of growth and damping is the superposition of many flat distributions uniformly distributed in $\log E$ and so is uniform (unless the thermal level and nonlinear threshold are allowed to be close together and to vary substantially from cycle to cycle). These arguments are not altered by allowing the growth and damping rates for each growth/damping cycle to be different in successive cycles (provided the rates are constant within a given cycle) since the $P(\log E)$ distribution for each cycle is still uniform.

Above the nonlinear threshold the $P(\log E)$ distribution predicted for uniform secular growth, and the evolution of the wave field, depends on the nature of the nonlinear process. Nonlinear exponential damping should leads to the uniform distributions described above. If instead a process like trapping causes the wave field to oscillate slowly about some asymptotic value above the nonlinear threshold (with exponential damping on much longer timescales), then the $P(\log E)$ distribution should be uniform below the nonlinear threshold but have a peak at higher fields near the asymptotic value. Finally, if the nonlinear process is a modulational instability or involves wave collapse then the $P(\log E)$ distribution should show a powerlaw tail above the nonlinear threshold (but be uniform below the threshold) [*Robinson and Newman*, 1990]. These cases are illustrated in Figure 2. In all cases, note that the uniform secular model predicts that the $P(\log E)$ distribution should be uniform below the nonlinear threshold field but that the distribution above the threshold depends on the active nonlinear process.

The time separation between neighboring field samples in most spacecraft experiments is typically long

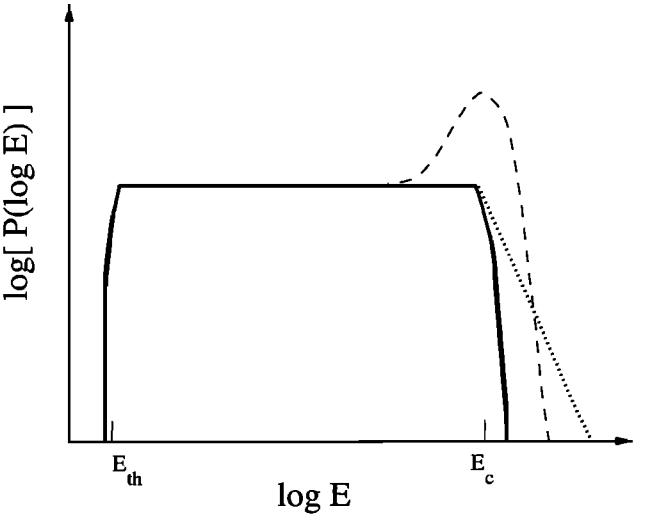

Figure 2. The distributions $P(\log E)$ predicted for the standard model with various nonlinear saturation mechanisms: the solid line shows the rigorous prediction for exponential linear growth and nonlinear damping, the dashed line shows the qualitative prediction for saturation about a field E_c, and the dotted line shows the qualitative prediction for when wave collapse is relevant above E_c.

compared with the inverse frequency and growth time of the waves, as for the PF waves here. Since the spacecraft typically moves through the plasma, this means that a wave packet of short-wavelength waves is usually only sampled once or a few times during its evolution, so that most field samples correspond to different wave packets. Meaningful analysis of wave and particle properties, including the wave statistics, then requires the standard experimental assumption that the properties of the wave-particle-plasma system vary only smoothly on macroscopic time and distance scales, with the wave-particle-plasma properties and statistics being well defined in data sets over shorter time intervals. The uniform secular growth model makes the stronger assumption of spatial homogeneity at all times, and the arguments above for data sampled uniformly or randomly in time imply that that this model predicts uniform $P(\log E)$ distributions for such spacecraft data. Even allowing the growth/damping rates to have different constant values from one cycle of wave growth to the next, without explicit justification but outside the basic model if the system parameters are constant, does not alter this conclusion. Testing SGT with spacecraft data requires only the assumption that the wave statistics are well defined over the measurement interval. Thus both SGT and the uniform secular model can be tested definitively using the observed $P(\log E)$ distribution.

Detailed analyses show that the bursty, widely varying, persistent Langmuir waves (more properly Langmuir-z mode waves) driven by electron beams in interplanetary type III solar radio burst sources are quantitatively consistent with SGT and with the electrostatic decay process $L \rightarrow L' + S$ being active above a few mV m^{-1} [*Robinson et al.*, 1993a,b]. (Here L and L' denote Langmuir-like waves and S denotes an ion sound wave, respectively.) Similar analyses demonstrate that pure SGT describes very well the Langmuir-like waves driven by electron beams in the majority of Earth's foreshock [*Cairns and Robinson*, 1997, 1999]. In comparison, the uniform secular model for wave growth is incontrovertibly inconsistent with these observations [*Robinson et al.*, 1993a; *Cairns and Robinson*, 1997, 1999] since the observed distributions are lognormal in E and not uniform below the nonlinear thresholds.

SGT predictions for the $P(\log E)$ distribution are also known for pure thermal waves and for thermal waves subject to both stochastic growth effects and steady driving by an instability [*Robinson*, 1995]. These predictions agree very well with observations of thermal Langmuir waves in the solar wind and with the driving of these thermal Langmuir waves by electron beams at the upstream edge of Earth's foreshock [*Cairns et al.*, 2000]. SGT thus already provides a quantitative theoretical explanation for both driven and thermal Langmuir wave phenomena (more properly, Langmuir/z phenomena [*Willes and Cairns*, 2000]) in four different plasma regions. These successes and the burstiness, widely varying fields, and persistence of PF waves imply that SGT is a natural theory to apply to PF waves.

3. Wave Data

This paper presents data from the step frequency receiver (SFR) and wideband receiver (WBR) of the plasma wave instrument (PWI) on the Dynamics Explorer 1 (DE 1) spacecraft. *Shawhan et al.* [1981] describe the PWI instrument in detail; only a brief summary is provided here of the SFR and WBR for AC electric fields. Every 32 s in the normal observational mode, the SFR steps through 128 logarithmically spaced, nonoverlapping channels covering the frequency range from 100 Hz to 400 kHz, one at a time. Each channel is very narrowband, with a bandwidth of 6 Hz from 100 to 800 Hz, 52 Hz between 0.9 and 6.4 kHz, and 480 Hz between 7.3 and 51.2 kHz.

The WBR measures the time-varying waveform on a designated antenna and in a designated frequency range (here 650 Hz to 40 kHz). Once digitized, the WBR data have excellent frequency resolution, usually $\sim$ 100 Hz. An automatic gain control (AGC) with a time constant of $\sim$ 0.5 s is used to maintain the signal within a set range of amplitudes for analog telemetry to the ground [*Shawhan et al.*, 1981]. The AGC voltage has discrete settings and is reported once per second, while the spacecraft spin period is 6 s. The AGC voltage thus measures the time-varying, integrated wave field on the antenna over the entire designated frequency range.

The period analyzed here is the one used originally to define PF waves [*Cairns and Menietti*, 1997]: 2231–2400 UT, day 208 (July 27), 1981. During this period, DE 1 was moving earthward at radial distances of $\sim 4.4\ R_E$ to $2.9\ R_E$ through the nightside, southern hemisphere, auroral region and polar cap. The bottom half of Plate 1, repeated from *Cairns and Menietti* [1997], is a color spectrogram of the electric field spectral density from the SFR. The top black curve, ranging from 20 to 80 kHz, represents the electron gyrofrequency f_g while the bottom two black curves below 100 Hz show the proton and oxygen gyrofrequencies.

PF waves are observed in Plate 1 (bottom) as the bursty, intense emissions (red and yellow colors) ranging from $\sim 3-6$ kHz near 2232 UT to $\sim 9-15$ kHz near 2345 UT [*Cairns and Menietti*, 1997]. These waves are quite narrowband, with $\Delta f/f \sim 0.3$ relative to their center frequency, and occur well below f_g at frequencies of order those expected for f_p at these altitudes. Analysis of a low-frequency feature in the WBR data for this interval, identified as the low-frequency cutoff of z mode waves, strongly implies that f_p lies in the range $6.1 - 8.0$ kHz for the period 2300–2308 UT and so spans the bandwidth of the PF waves [*Cairns*, 1999]. The lower-amplitude (green), less bursty waves at frequencies below the PF waves but above 1 kHz are identified as whistler mode hiss propagating from an auroral source [*Cairns and Menietti*, 1997], on the basis of

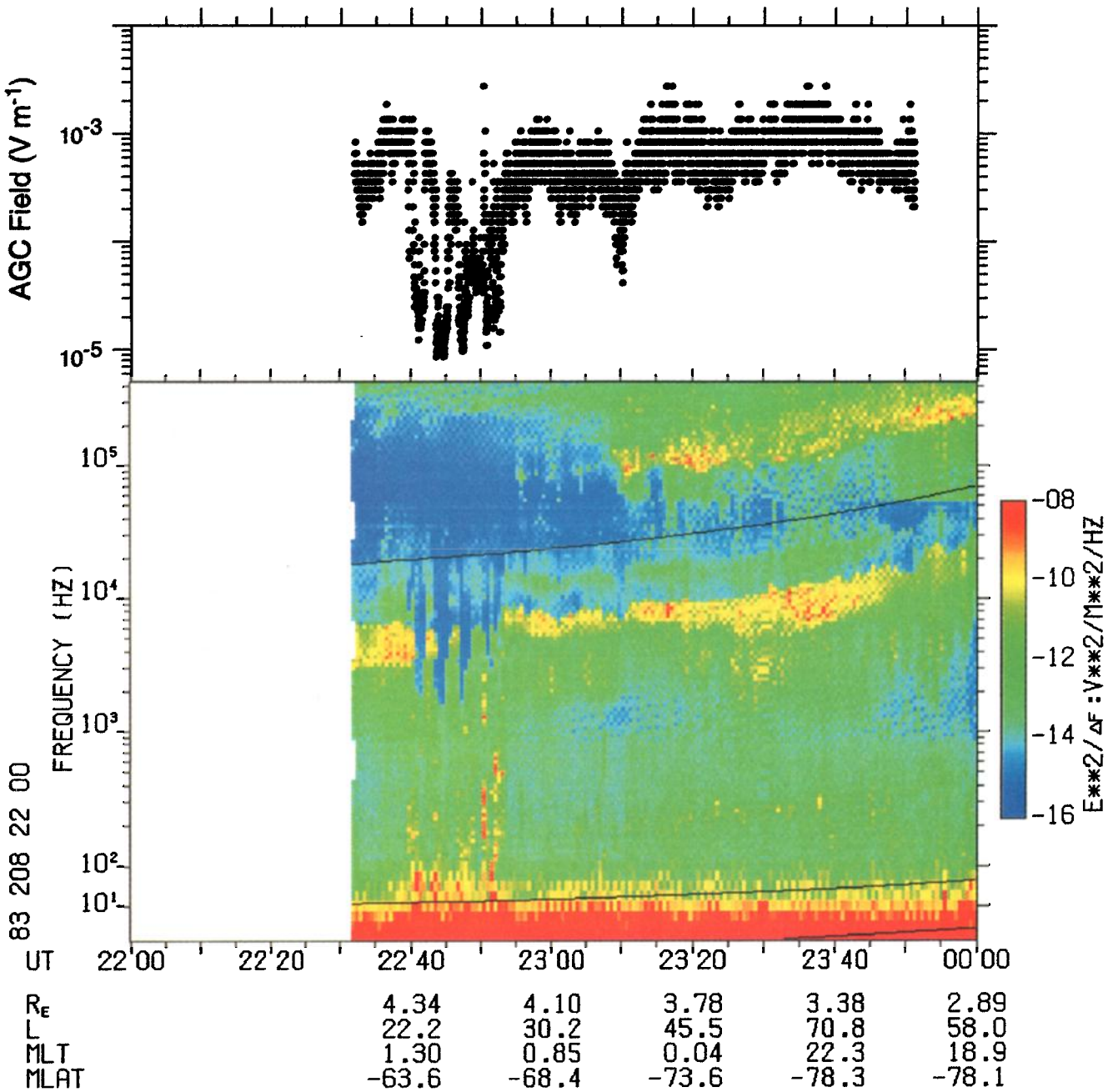

Plate 1. DE 1 plasma wave data for 2200–2400 UT on July 27, 1983: (top) AGC fields; (bottom) SFR dynamic spectrum with the electric spectral density color coded.

work by *Gurnett et al.* [1983] and *Persoon et al.* [1983, 1988]. Also present are the H component, which is the weak emission at twice the frequency of the PF band (interpreted as z mode waves) [*Cairns and Menietti,* 1997; *Menietti et al.,* 1998], auroral kilometric radiation (AKR) at frequencies above $\sim$ 100 kHz [*Gurnett,* 1975], bursty waves at $\sim 10 - 1000$ Hz in the auroral region, and the new class of low frequency waves in the range $100 - 600$ Hz after about 2300 UT, which are the focus of section 5. The auroral region (2240–2255 UT) is marked by the presence of auroral plasma cavities, which lead to the disappearance of the PF waves, the reduction of the maximum frequency extent of the hiss emissions, and intense bursts of the waves from $\sim$ 10 Hz to 1 kHz.

Plate 1 (top) shows the AGC level of the WBR, sampled once per second, after converting into the equivalent electric field using calibration data and the effective antenna length. The discreteness of the AGC levels is evident. Since the PF waves clearly have much larger spectral densities and relatively broad bandwidths compared with the other waves observed below 40 kHz (the upper cutoff of the WBR), then the AGC field is to a good approximation the field of the PF waves at that time. Since the AGC voltage is sampled once per second, while the SFR sweeps through the PF band only every 32 s and uses very narrowband channels, the electric field calculated from the AGC voltage is a rapid and accurate way to measure the total electric field of the PF waves. Importantly, the AGC data are clearly organized into a relatively broad band which moves as a unit up and down in time. This provides immediate, strong evidence for an intrinsic distribution of wave fields, as expected for SGT. Of some concern below is the potential for these temporal movements of the band of AGC fields to modify the intrinsic $P(\log E)$ distributions, especially well away from the peak of the distribution.

Comparison of the AGC fields and the spectrogram in Plate 1 shows that the AGC fields rise where the spectrogram shows intense waves and decrease where the PF waves are weaker or absent, particularly during the interval 2240–2255 UT when auroral plasma cavities were traversed. The AGC electric fields are also quantitatively consistent with those estimated by taking spectral densities from Plate 1, multiplying by the channel bandwidths (see above), and taking the square root. More detailed comparisons of the AGC fields with spectrograms of WBR data are given in Plates 2 and 3 of *Cairns and Menietti* [1997] and are not repeated here. The only additional comment made now is that some periods of hiss are mislabeled as PF waves in Cairns and Menietti's Plate 2 because of the WBR's low-frequency rolloff combining with the monotonically decreasing hiss spectrum to yield an apparent signal near 1–2 kHz that mimicked PF waves in the WBR data. In particular, on the basis of the spectral profile and wave intensities in Plate 1's SFR data, the periods 2246:50–2247:45, 2248:00–2248:20, 2250:20–2251:10, and 2251:40–2252:50 UT are dominated by hiss. It is worth pointing out that periods with hiss sometimes have AGC fields that are as large as those for PF periods and that these AGC fields are not constant but instead vary substantially with time.

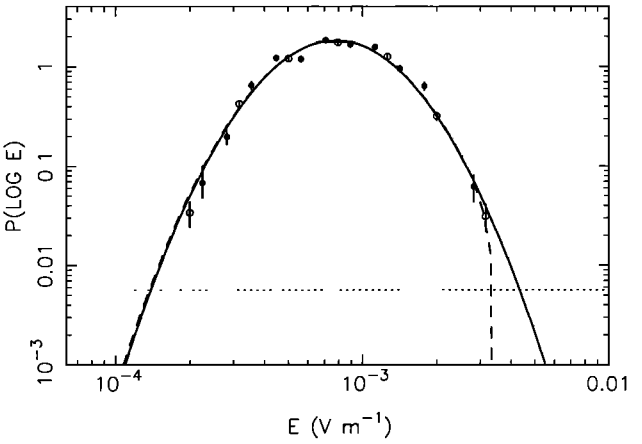

Figure 3. The observed distribution $P(\log E)$ for 5 and 10 bins per decade in $\log E$ is displayed for the period 2320–2350 UT on July 27, 1983, using open and solid circles, respectively. Solid and dashed lines show the best fits to the SGT predictions (3) and (4) for the observed distribution with 5 bins per decade in $\log E$. The parameters and statistical significance of the fits are summarized in Table 1. The dotted line shows the two-sample line.

4. Application of SGT to PF Waves

Figure 3 displays the $P(\log E)$ distribution of PF waves for the period 2320–2350 UT, calculated by binning the time series of AGC fields with 5 or 10 bins per decade in $\log E$ (open and solid circles, respectively) and then normalizing so that

$$\int d(\log E)\ P(\log E) = 1\ . \tag{6}$$

This period is chosen because the PF waves continue uninterrupted for a long period and the AGC fields remain in a reasonably constant range, thereby providing a large number of field samples for analysis, albeit with a large change in the frequency of the PF waves and altitude range of the spacecraft and some oscillations in the band of AGC fields. The error bars on the values of $P(\log E)$ for each bin are calculated using $\pm\sqrt{N}$ estimates, where N is the number of samples in each bin of $\log E$. The dotted line represents the two-sample line; in this paper only bins with more than two samples are used in the χ^2 minimization procedures. Comparison with Figure 1 and the SGT prediction (3) immediately shows that the data are in very good qualitative agreement with SGT but are clearly inconsistent with the secular growth model.

The solid line in Figure 3 quantifies the agreement between the SGT prediction and the $P(\log E)$ distribu-

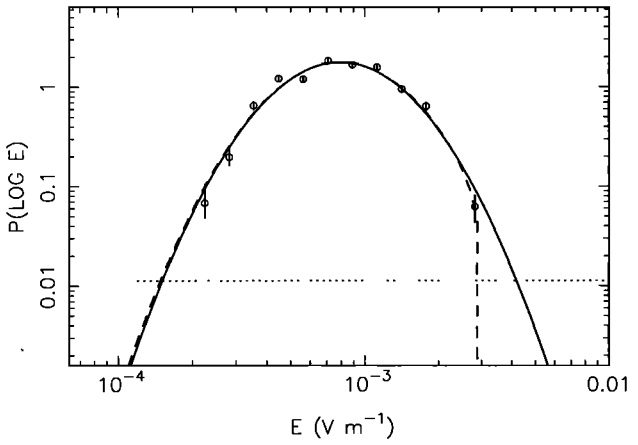

Figure 4. The observed distribution $P(\log E)$ with 10 bins per decade in $\log E$ for the same interval in Figure 3 is compared with best fits to the SGT predictions (3) and (4) using solid and dashed lines, respectively. The dotted line shows the two-sample line.

tion with 5 bins per decade in $\log E$, being the best fit to the pure SGT prediction (3) obtained using a geometric simplex method [*Press et al.*, 1986] to minimize χ^2 between the predicted and observed number of samples in each bin of the $P(\log E)$ distribution. Visual observation shows that the $P(\log E)$ distributions for 5 and 10 bins per decade are in good quantitative agreement with each other and the SGT fit to (3). Table 1 presents the fit parameters and the formal statistical goodness of the fit. There, $\chi^2 = 9.1$ for 7 bins but 4 degrees of freedom, the reduced χ^2 is 2.3, and the significance probability $P(\chi^2) = 0.06$ [*Press et al.*, 1986]. As is conventional, the number of degrees of freedom equals the number of bins minus the number of fit parameters (two here) minus one (since the predicted distribution is normalized to the number of samples), while $P(\chi^2)$ is the probability of obtaining, by chance, a larger value of χ^2 even if the model is correct. (Higher values of $P(\chi^2)$, < 1 by definition, correspond to higher statistical significance.) Accordingly, there is good quantitative and statistical agreement between these data and the predictions of pure SGT.

The $P(\log E)$ distribution plotted in Figure 4 is the distribution with 10 bins per decade from Figure 3; now, however, the solid curve is the best fit to (3) for these data. Once again, good qualitative and semiquantitative agreement is apparent between pure SGT and the data. Table 1 shows, moreover, that fitting the pure SGT prediction (3) to these two distributions yields almost identical fit parameters. For the 10 bin per decade distribution, however, the normalized χ^2 value is larger, and the significance probability $P(\chi^2)$ is much lower.

As described in section 2, the $P(\log E)$ distribution can also be used to investigate whether a nonlinear process is active at high E. Qualitatively, Figures 3 and 4 suggest that the $P(\log E)$ distributions for this long interval fall off somewhat more quickly at high E above a few mV m^{-1} than expected for pure SGT, thereby providing weak qualitative evidence for a nonlinear process removing energy from the waves there. On the other hand, the $P(\log E)$ distributions also fall off somewhat more rapidly at small $E \lesssim 3 \times 10^{-4}$ V m^{-1} than predicted, pointing to another effect being at work. Thermal noise effects [*Robinson*, 1995; *Cairns et al.*, 2000] cause the distribution to increase at low E, not decrease, and so are not being observed here. The dashed lines in Figures 3 and 4 quantify this evidence for a nonlinear process by plotting the fits to the nonlinear SGT prediction (4), obtained by minimizing χ^2 using the geometric simplex method. The fit parameters and statistical quantities are given in Table 1. In both figures the fits to nonlinear SGT slightly better describe the $P(\log E)$ distribution at high E, retain the good agreement with linear SGT at fields below the derived nonlinear threshold, yield fit parameters that agree within the error bars, reduce χ^2, and have either slightly improved or similar significance probabilities. These properties provide weak evidence for an active nonlinear process at fields $\gtrsim 2$ mV m^{-1}.

The existence in Plate 1 of temporal trends up and down of the band of AGC fields, which have been averaged over for the interval 2320–2350 UT discussed thus far, might lead to modifications of the intrinsic $P(\log E)$ distributions. These modifications are most likely far from the distribution's peak, in bins with small numbers of field samples at low or high $\log E$, but could also occur near the peak of the distribution. Both effects would increase χ^2 and decrease the statistical significance of the fits. Two ways to reduce these effects are (1) to remove the trends in μ and σ by analyzing the distribution $P(X)$ of the de-trended variable $X = (\mu - \log E)/\sigma$, as done successfully elsewhere for foreshock waves [*Cairns and Robinson*, 1999], or (2) to analyze shorter intervals for which the trends are smaller. The second course of action is followed in this paper, despite the smaller number of samples available for analysis.

Figure 5 shows the distribution $P(\log E)$ for the shorter interval 2255–2305 UT, for which the PF waves are present continuously with almost constant frequency and the band of AGC fields varies relatively little. The best fits to predictions (3) and (4) for pure and nonlinear SGT are displayed using solid and dashed lines, respectively, and are summarized in Table 1. For this interval the $P(\log E)$ distribution is well described qualitatively and semiquantitatively by pure SGT at fields below a few mV m^{-1} but with significant evidence for a nonlinear process at higher fields. The nonlinear fit has good statistical significance. Once again, the observed $P(\log E)$ distribution is inconsistent with the secular growth model.

Even during the brief episodes of PF waves between when DE 1 moves through auroral plasma cavities, the $P(\log E)$ distributions are qualitatively and semiquantitatively consistent with SGT. This is shown in Figure 6 for the interval 2236–2239 UT. The best fits to (3)

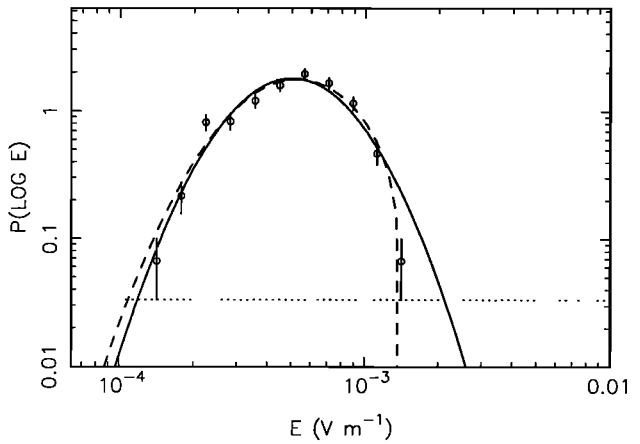

Figure 5. The observed $P(\log E)$ distribution for the period 2255–2305 UT is compared with SGT in the same format as Figure 4.

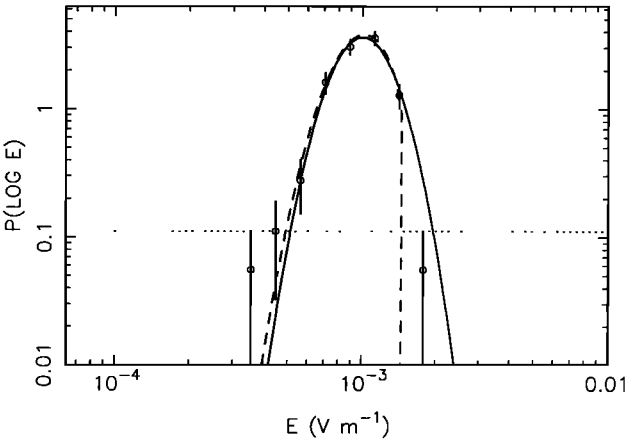

Figure 6. As for Figures 4 and 5 but for the period 2236–2239 UT.

and (4) are displayed using the solid and dashed lines, respectively; very good agreement is evident. Moreover, despite the small number of field samples ($\leq$ 180) for the distribution, χ^2 is small (Table 1), and the significance probabilities for the fits are very high ($\gtrsim$ 0.4).

Finally, Figure 7 shows the $P(\log E)$ distribution for the interval 2257–2259 in which PF waves are present continuously and the AGC band is almost stationary in time. The fits to both (3) and (4) agree very well with the data and are strongly statistically significant, especially the nonlinear fit (4). This provides strong evidence that SGT is relevant, that a nonlinear process operates at fields $\gtrsim$ 1 mV m^{-1}, and that the secular growth model does not apply.

5. Possible Nonlinear Product Waves

Inspection of Plate 1 reveals the presence of a band of waves at low frequencies $\sim 150 - 400$ Hz from $\sim$ 2310–2350 UT. This band moves upward in frequency with time and is composed of bursty waves, thereby mimicking the PF band in these two respects. These characteristics are qualitatively consistent with the waves being produced in the nonlinear process inferred from the $P(\log E)$ distributions of the PF waves at high fields.

Interpreting these waves in terms of a nonlinear three-wave decay process, represented schematically as PF $\rightarrow$ LF + PF′ for two PF waves and a low-frequency (LF) quantum, then the following characteristics are expected by analogy with similar decay processes for Langmuir waves [e.g., *Robinson et al.*, 1993a, 1993b; *Cairns*, 1995]: (1) each participating triple of waves conserves frequency and wave vector (energy and momentum, respectively), (2) larger PF fields should lead to larger LF fields, ideally being linearly proportional, and (3) LF waves should be produced only when the PF field is above the threshold for the nonlinear process.

Unfortunately, the SFR data in Plate 1 are not well suited for testing these predictions because of the long sweep time (32 s) required to sample the entire spectrum, the large number of nonsimultaneously sampled SFR channels, the small number of spectra (74) for this interval, and the rapid burstiness of the PF waves (on timescales $\lesssim$ 1 s according to both the WBR and SFR data in Plate 1). One reason is that the SFR does not report simultaneous fields for both the PF waves and any LF product waves, since it samples only one channel at a time, thereby preventing a direct and accurate test of the predictions. In particular, the stepping nature of the SFR instrument means that the LF field associated with an unsampled but large PF field will

Table 1. SGT Fit Parameters for Equations (3) and (4)

Period, UT	Figure	Equation	Bins	μ	σ	$\log E_c$	N	χ^2	$P(\chi^2)$
2320–2350	3	(3)	5	-3.1 ± 0.1	0.22 ± 0.02	–	4	9.1	0.06
2320–2350	3	(4)	5	-3.1 ± 0.1	0.22 ± 0.02	-2.5 ± 0.2	3	7.7	0.05
2320–2350	4	(3)	10	-3.1 ± 0.1	0.23 ± 0.02	–	8	35	3×10^{-5}
2320–2350	4	(4)	10	-3.1 ± 0.1	0.23 ± 0.02	-2.5 ± 0.2	7	32	5×10^{-5}
2255–2305	5	(3)	10	-3.3 ± 0.1	0.22 ± 0.02	–	8	28	5×10^{-4}
2255–2305	5	(4)	10	-3.3 ± 0.1	0.24 ± 0.02	-2.8 ± 0.4	7	16	0.03
2236–2239	6	(3)	10	-3.0 ± 0.1	0.11 ± 0.02	–	2	1.3	0.5
2236–2239	6	(4)	10	-2.8 ± 0.2	0.12 ± 0.04	-2.8 ± 0.3	1	0.8	0.4
2257–2259	7	(3)	10	-3.2 ± 0.1	0.16 ± 0.02	–	4	6.3	0.2
2257–2259	7	(4)	10	-3.1 ± 0.1	0.20 ± 0.02	-2.8 ± 0.2	3	3.5	0.3

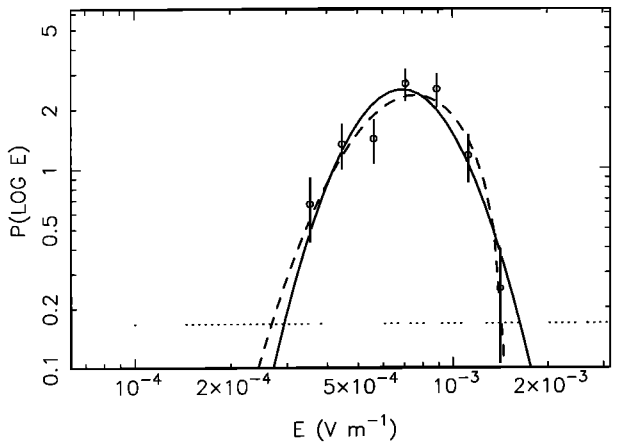

Figure 7. As for Figures 4–6 but for the period 2257–2259 UT.

usually be grouped with an uncorrelated and typically lower PF field (since only a very small fraction of PF fields are within a factor of 2 of the nonlinear thresholds in Figures 3–7). This will smear out any correlation and introduce a large scatter to the results. Second, the small number of spectra available (74) and large number of SFR channels (128) lead to small probabilities of properly associating correlated signals. For example, if the LF and PF waves occur in a single constant amplitude pulse located randomly in time once every 32-s spectra, then there is only a 1/128 chance of observing the LF pulse in any one SFR spectra and only a chance of 74/128 ≈ 60% of sampling an LF pulse over the entire interval. Overwhelmingly, then, LF product waves will be inadequately sampled and related to the PF waves driving them. This situation is made even worse by the variations in the average field of the PF waves visible in Plate 1.

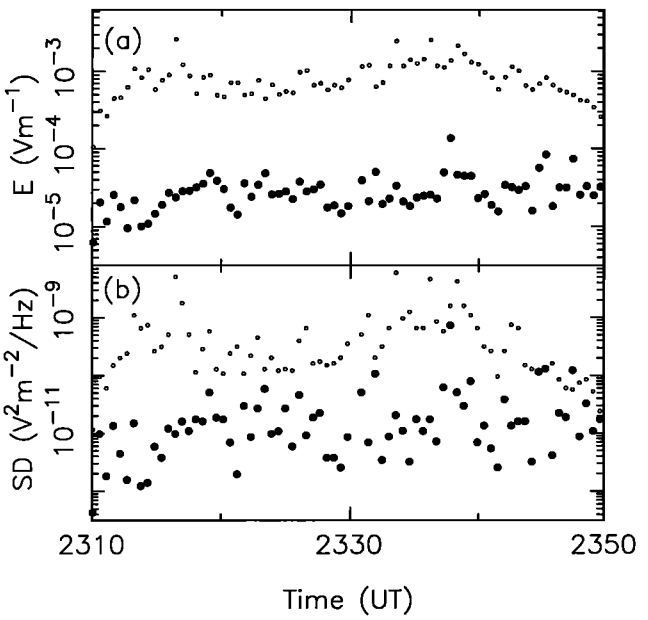

Figure 8. The properties of PF and LF waves are compared as a function of time using open and solid circles, respectively: (a) electric fields integrated over the bands for each sampled SFR spectrum, (b) the maximum spectral densities in each band of the SFR spectrum.

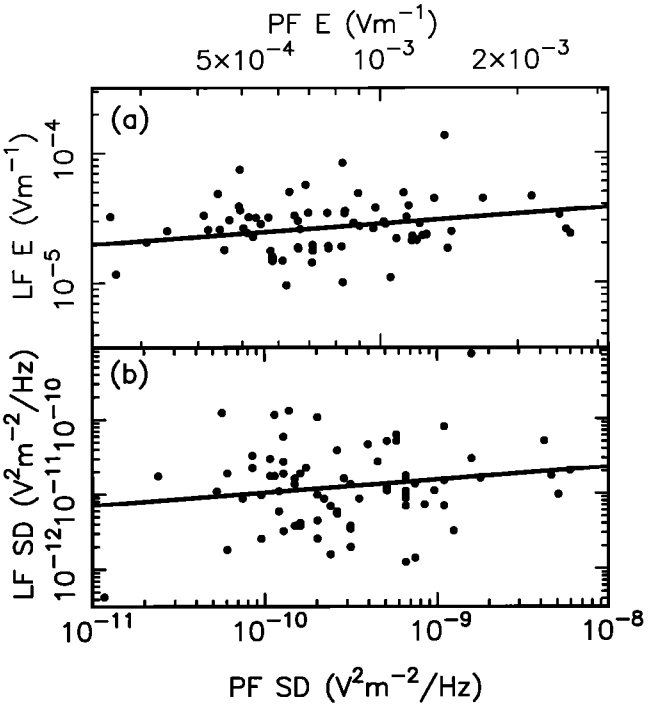

Figure 9. Scatterplots and associated powerlaw fits to equation (8) (solid line) are used to quantify relationships between the PF and LF waves: (a) electric fields integrated over the bands, (b) the maximum spectral densities in each SFR spectrum.

Figure 8a compares the total electric fields of the PF and LF bands as a function of time, estimated by integrating the measured SFR spectral densities over the ranges 5–20 kHz and 150–400 Hz for each spectrum, respectively. Figure 8b shows the maximum spectral densities in each band as a function of time. With only 74 points in each band, the statistics are poor. However, visual inspection suggests a possible weak correlation.

Figures 9a and 9b are scatter plots with superposed fits that quantify correlations between the LF and PF waves for Figures 8a and 8b, respectively. The lines are obtained by standard least squares minimization of the data to the powerlaw expression

$$y = A\, x^{\alpha} \,. \tag{7}$$

Here x and y are the total electric field or maximum spectral density in the PF band (x) and LF band (y), respectively. Table 2 contains the parameters and statistical significance of these fits. In each case, there is a weak positive correlation, with $\alpha > 0$, between the PF and LF fields. However, the expected index for a three-wave process is $\alpha = 1$ [*Robinson et al.*, 1993b; *Cairns*, 1995], quantitatively inconsistent with the fits More-

Table 2. Fit Parameters to Equation (8)

Quantities	α	$\log_{10} A$	χ^2	$P(\chi^2)$
Fields	0.25 ± 0.10	-3.8 ± 0.3	78	0.29
SD	0.17 ± 0.11	-9.3 ± 1.1	84	0.16

over, the LF waves appear to be associated with PF waves over a broad range of PF fields and spectral densities, including fields a factor ≈ 5 smaller than the nonlinear thresholds estimated in section 3 from the $P(\log E)$ distributions. These difficulties are not unexpected given the systematic effects described above.

In summary, the SFR data show the presence of low-frequency waves whose qualitative characteristics are not inconsistent with their production in a nonlinear process involving PF waves, but quantitative analysis yields only inconclusive evidence in favor of this interpretation. For the reasons given above, the lack of supporting evidence is not unexpected. Even so, these analyses provide weak support for the interpretation reached in section 4 that the PF waves undergo a nonlinear process at high fields. Further work on the mode of the low-frequency waves and the identity of the nonlinear process is required.

6. Explanation for Why an SGT State is Attained

Demonstrating that the observed wave statistics follow the functional form predicted by SGT is only the first part of constructing a detailed SGT description of the waves and driving particle distribution. The second part is to develop a detailed model for why an SGT state is attained. Analytic versions of such models exist for Langmuir-like waves driven by electron beams in interplanetary type III solar radio burst sources and in Earth's foreshock [*Robinson et al.*, 1993a; *Cairns and Robinson*, 1997]. Here, by modifying these models, we construct an analytic model for why PF waves attain an SGT state.

The model assumes that PF waves are driven by electron beams, with beam speeds v_b ranging from 1 to 10 electron thermal speeds V_e, in an inhomogeneous plasma containing MHD turbulence. Observations by J. D. Dorelli et al. (unpublished manuscript, 2000) support the existence of electron streams over the polar cap (at altitudes $\sim 7\ R_E$) with bulk speeds $\sim (1-5) \times 10^6$ m s^{-1} and thermal speeds of similar order, with pitch angle properties suggesting an origin at low altitudes. This paper's DE 1 observations took place at much lower altitudes $\sim 1-3\ R_E$, where V_e is believed much smaller ($\approx (1-10) \times 10^5$ m s^{-1}) [*Menietti and Burch*, 1985], so that the local ratio v_b/V_e can be significantly larger than 1. Similarly, the existence of turbulent MHD density irregularities in the inner magnetosphere is well known [e.g., *Persoon et al.*, 1983, 1988; *LeDocq et al.*, 1994]. A further assumption of the model is that the PF waves are driven resonantly on the beam mode [*Gary et al.*, 2000; *Willes and Cairns*, 2000]; this means that the group speed $v_g = |\partial\omega/\partial\mathbf{k}|$ equals v_b. Relaxing this assumption by having the waves grow on the Langmuir/whistler or z modes will reduce v_g, because these modes have smaller dispersion than the beam mode in the unstable region, and thereby will further improve the applicability of the SGT model, as shown below.

The model developed next, for electron beam-driven PF waves attaining an SGT state, follows very closely those developed for Langmuir waves driven by electron beams in type III burst sources and Earth's foreshock [*Robinson et al.*, 1993a; *Cairns and Robinson*, 1997]. Consider PF waves growing in the inhomogeneous background plasma in a growth site with characteristic size $\langle l \rangle$. The waves remain in this region for a time

$$t_g = \langle l \rangle / v_g = \langle l \rangle / v_b \ . \tag{8}$$

During this time, portions of the beam from within a distance $v_b t_g$ pass through the growth site, traversing a number $N_1 = v_b t_g / \langle l_{\rm sep} \rangle$ of growth sites, where $\langle l_{\rm sep} \rangle$ is the average separation distance of the growth sites. In each growth site the beam drives waves, thereby partially quasi-linearly relaxing the beam and injecting fluctuations into the beam distribution. Importantly, the growth sites are not time stationary but instead evolve on the MHD timescale, with a lifetime

$$t_A = \langle l \rangle / V_A \ , \tag{9}$$

where V_A is the Alfven speed. Accordingly, the total number of fluctuations injected into the beam during the time t_g is

$$n_{fl} = N_1 \frac{t_g}{t_A} = \frac{v_b t_g^2}{\langle l_{\rm sep} \rangle t_A} \ . \tag{10}$$

Assuming beam mode waves, this reduces to

$$n_{fl} = \frac{\langle l \rangle}{\langle l_{\rm sep} \rangle} \frac{V_A}{v_b} \ . \tag{11}$$

The characteristic duration of these beam fluctuations is then

$$t_i = t_g / n_{fl} = t_A / N_1 = \langle l_{\rm sep} \rangle / V_A \ . \tag{12}$$

These expressions differ from previous models only in their consideration of MHD rather than gasdynamic evolution of the turbulence, retention of $\langle l_{\rm sep} \rangle$ and $\langle l \rangle$, and the beam mode assumption made in the final expressions. The first of these differences is vitally important in the polar magnetosphere, since V_A greatly exceeds the ion acoustic speed V_S, but is unimportant in the solar wind (where $V_A \approx V_S$ usually).

For the PF event analyzed here, $f_g \approx 10$ kHz and $f_p \approx 5$ kHz, implying a magnetic field ~ 350 nT and

number density ~ 0.3 cm^{-3}. The electron temperature T_e was not measured, but values ~ 5000 K appear typical based on DE observations [*Menietti and Burch*, 1985]. For these parameters, $V_A \approx 1.2 \times 10^7$ m s^{-1}, $V_S \approx 10^4$ m s^{-1} for equal proton and electron temperatures, and $V_e \approx 3 \times 10^5$ m s^{-1}. Assuming that the MHD turbulence fills the plasma, then $\langle l \rangle \approx \langle l_{\rm sep} \rangle$ and

$$n_{fl} \approx V_A/v_b \approx 40 V_e/v_b \ . \tag{13}$$

Thus $n_{fl} \gg 1$ for $v_b \lesssim 5V_e$, many beam fluctuations pass through a growth site during the time t_g and the Central Limit Theorem can be expected to apply. This explains why the SGT predictions (3) and (4) apply and agree so well with the available data. For faster beams the assumption $v_g = v_b$ used in deriving (14) is likely poor; this is because faster beams tend to be relatively dilute, so that growth occurs on the Langmuir/whistler mode (not the beam mode) [*Gary et al.*, 2000; *Willes and Cairns*, 2000], v_g is substantially less than v_b, and n_{fl} is increased by the ratio v_b/v_g. This factor is large for Langmuir waves in type III solar radio burst sources [*Robinson et al.*, 1993a].

The proton gyroradius is ~ 200 m for these parameters. In comparison, assuming that the clump lifetime t_g is 1 s, not inconsistent with Plate 1, (8) implies that

$$\langle l \rangle \approx 300 \text{ km} \tag{14}$$

for $v_b = V_e = 3 \times 10^5$ m s^{-1}. This length scale is not unreasonable and falls well within the range expected for MHD turbulence expected at these altitudes. Substituting this value into (12), the predicted duration of the beam fluctuations is

$$t_i \approx 2.5 \times 10^{-2} \text{ s} \ . \tag{15}$$

In comparison, for $v_b = 5V_e$, $\langle l \rangle = 60$ km, and $t_i = 5 \times 10^{-3}$ s. These predicted durations are much smaller than the measurement timescale of most existing electron detectors, which are typically $\gtrsim 3$ s.

Calculating the mean time-varying energy of the waves (by averaging over the distribution $P(G)$ via $< E^2(t) > = \int dG\ e^{G(t)} P(G)$) and then making the SGT assumption that the system is near marginal stability (time- and volume-averaged) yields a relationship between the mean $\langle \Gamma \rangle$ and standard deviation $\sigma(\Gamma)$ of the (energy) growth rate of waves [*Robinson et al.*, 1993a]:

$$\langle \Gamma \rangle = -\sigma^2(\Gamma) t_i/2 \ . \tag{16}$$

Equation (16) explains qualitatively how waves can grow effectively despite a large mean damping rate and how the system remains near marginal stability: relatively large values of $\sigma(\Gamma)$ allow significant wave growth on timescales of several t_i in a small proportion of the plasma to be balanced by wave damping in the majority of the plasma. Equation (16) also allows the relative burstiness of the waves to be predicted and compared with observations [*Robinson et al.*, 1993a; *Cairns and Robinson*, 1997], as performed next for PF waves.

The average (energy) growth rate $\langle \Gamma \rangle$ of PF waves is approximated here by ignoring the effects of the beam electrons and using the damping rate of Langmuir waves on a Maxwellian distribution of background electrons. Analytic theory then yields [e.g., *Stix*, 1962; *Krall and Trivelpiece*, 1973]

$$\langle \Gamma \rangle = -\sqrt{2\pi} \left(\frac{v_\phi}{V_e} \right)^3 e^{-v_\phi^2/2V_e^2} \ \omega_p \ , \tag{17}$$

where v_ϕ is the wave phase speed. For $v_\phi = v_b = V_e$ and $f_p = 5$ kHz, $\langle \Gamma \rangle = -5 \times 10^4$ rad s^{-1}. Substituting $t_i = 25$ ms from (15), (16) then implies

$$\sigma(\Gamma) \approx 2 \times 10^3 \text{ rad s}^{-1} \ . \tag{18}$$

Thus the ratio $\sigma(\Gamma)/\langle \Gamma \rangle = -0.04$. This suggests that the fluctuations in Γ should be quite small. Assuming instead that $v_\phi = v_b = 5\ V_e$ leads to $\langle \Gamma \rangle \approx 50$ rad s^{-1}, $\langle l \rangle = 60$ km, $t_i = 5$ ms, $\sigma(\Gamma) = 10$ s^{-1}, and $\sigma(\Gamma)/\langle \Gamma \rangle \approx 0.2$, implying burstier waves. Thus the burstiness of the waves should depend quite strongly on v_b, $\langle l \rangle$, V_A, and $\langle \Gamma \rangle$. Direct comparisons between the model and observations (since growth rates are not directly measurable from the DE wave data, unlike the wave fields and gains) involve a change in variables.

The gain G, which equals the total number of e-foldings, of a clump of waves is the sum over the individual increments $\Delta G \approx \Gamma t_i$ of all beam fluctuations passing through during the time t_g, where Γ is a function of time. It can be shown [*Robinson et al.*, 1993a] that $\langle G \rangle = \langle \Gamma \rangle t_g$ and $\sigma^2(G) = \sigma^2(\Gamma) t_i t_g$. These relations imply that

$$\frac{\sigma(G)}{\langle G \rangle} = \frac{\sigma(\Gamma)}{\langle \Gamma \rangle} \left(\frac{t_i}{t_g} \right)^{1/2} \ . \tag{19}$$

The observed quantities $\mu = \langle \log_{10} E \rangle$ and $\sigma = \sigma(\log_{10} E)$ are related to $\langle G \rangle$ and $\sigma(G)$ by $\langle G \rangle = -2 \ln 10\ \langle \log E \rangle + 2 \ln E_0$ and $\sigma(G) = 2\sigma \ln 10$. Choosing $E_0 = 1$ V m^{-1},

$$\frac{\sigma}{\mu} = \frac{\sigma(G)}{\langle G \rangle} \ . \tag{20}$$

Combining (19) and (20), the SGT model predicts that

$$\frac{\sigma}{\mu} = \frac{\sigma(\Gamma)}{\langle \Gamma \rangle} \left(\frac{t_i}{t_g} \right) = \frac{\sigma(\Gamma)}{\langle \Gamma \rangle} \left(\frac{v_g^2}{v_b V_A} \right)^{1/2} \ . \tag{21}$$

Assuming that $v_g = v_b = V_e$ and inserting the above values for V_A and the ratio $\sigma(\Gamma)/\langle \Gamma \rangle$ then yields $\sigma/\mu = -0.006$. If instead $v_b = 5V_e$, then $\sigma/\mu = -0.07$.

The values of μ and σ in Table 1, obtained by fitting the observed $P(\log E)$ distributions to the SGT predictions (3) and (4), imply that $\sigma/\mu = -0.07 \pm 0.01$. Comparing the observed and predicted values for μ/σ, the present analytic model can account for the burstiness of

the observed waves. One proviso is that the beams are relatively fast, with $v_b \approx 5V_e$ for the assumed plasma parameters.

Before summarizing the model, one final point is in order: ideally the prediction for σ/μ depends on fewer parameters than is apparent from (19) and (21). In particular, inserting the marginal stability relation (16) into (19) or (21) leads to

$$\frac{\sigma}{\mu} = \left(\frac{-2}{\langle\Gamma\rangle\, t_g}\right)^{1/2}, \qquad (22)$$

with no dependence on V_A or assumptions about the ratio v_g/v_b. That is, as measured by the ratio σ/μ, the relative burstiness of the waves depends only on two theoretical quantities: $\langle\Gamma\rangle$ and $t_g = \langle l\rangle/v_g$. Unfortunately, however, neither of these quantities is directly measured for the data set in this paper. Nevertheless, the measured ratio $\sigma/\mu = 0.07 \pm 0.01$ then implies that the product $\langle\Gamma\rangle\, t_g \approx -400$ rad s^{-1}.

The foregoing model is thus a viable theoretical explanation for why PF waves should attain an SGT state at DE 1 altitudes for electron beams with speeds commensurate with those observed by Polar at much higher altitudes. In particular, the model predicts that $n_{fl} \gg 1$, that the timescale for individual fluctuations in the beam is below current measurement capabilities, and that the burstiness of the waves should be of order that observed. Moreover, the sensitivity of the SGT predictions for n_{fl} and σ/μ to changes in $\langle\Gamma\rangle$, t_g, v_b, V_A, and V_e may potentially explain why PF waves are relatively rare in *Meniett i et al.*'s [1998] survey. First, events for which SGT is relevant but σ/μ is small will appear to have a smoothly varying, nonbursty wave spectrum and might not be identified as PF waves. Second, perhaps PF waves are rare because they are only observed when and where the beam and plasma parameters are suitable for the SGT constraints above to be attained. No detailed attempt is made here to describe the SGT state as a function of altitude or beam parameters nor to identify the nature of the growth sites (i.e., are they regions of decreased plasma density, minimal density gradient, etc.?). These matters are deferred to future work.

7. Discussion

The foregoing analyses show that the observed wave statistics are in good quantitative agreement with the functional form predicted by SGT and that a viable analytic model exists for why an SGT state should be attained. The detailed agreement between the wave statistics and SGT predictions for driven waves means immediately that the observed waves are being driven locally; this implies the existence of electron beams local to the spacecraft in a state close to time- and volume-averaged marginal stability. Since the PF event analyzed here is relatively typical, this means that the presence of PF waves can be routinely used to infer the presence of local electron beams. The survey analysis of *Meniett i et al.* [1998], which shows PF waves occurring over a broad range of altitudes $\sim 1 - 4\ R_E$, magnetic latitudes (for the polar cap and auroral region), and all magnetic longitudes (but particularly those near local midnight), thus suggests that previously undetected electron beams are present there. The existence of electron beams near marginal stability in these regions has not been previously inferred. The analyses of J. D. Dorelli et al. (unpublished manuscript, 2000) provide independent but direct support for this interpretation at higher altitudes $\gtrsim 7\ R_E$. The origin of these beams at polar cap latitudes, where no electron accelerator is known, needs detailed future consideration.

The polar cap represents a new location with very different plasma characteristics in which SGT applies. In particular, compared to previous SGT analyses of waves in the solar wind and Earth's foreshock [*Robinson et al.*, 1993a,b; *Cairns and Robinson*, 1997, 1999; *Cairns et al.*, 2000], at these altitudes the polar cap plasma is strongly magnetized ($f_g \gtrsim f_p$) rather than almost unmagnetized ($f_p \gg f_g$) and much colder ($T_e \lesssim 10^4$ K rather than $T_e \gtrsim 10^5$ K). SGT states can therefore develop in a wide range of plasmas.

As described in section 1, while PF waves are generated near f_p they are quite likely not generated in the Langmuir/z mode analyzed in the solar wind and terrestrial foreshock analyses [*Robinson et al.*, 1993a; *Cairns and Robinson*, 1997, 1999; *Cairns et al.*, 2000] Instead, these waves may have a strong beam mode component and are likely generated on the Langmuir/whistler mode, maybe even having a whistler component. Thus, in combination with these other analyses the present paper demonstrates that SGT applies in plasmas with widely different temperatures and magnetizations and to different wave modes. Moreover, SGT is observed to apply in all five cases analyzed observationally thus far (Langmuir waves and type III sources in the solar wind, thermal Langmuir waves in the solar wind, driven thermal waves at the foreshock's edge, Langmuir waves in the majority of the foreshock, and PF waves over Earth's polar cap), and it is predicted theoretically to be relevant in two other contexts, type III sources in the corona [*Cairns and Robinson,* 1998; *Robinson and Benz,* 2000] and low-frequency magnetosonic waves driven by interstellar pickup ions in the polar solar wind [*Zank and Cairns,* 2000]. These successes strongly suggest that SGT is widely applicable in space physics and, by extension, in astrophysics.

8. Conclusions

This paper demonstrates that SGT can account well for the detailed functional form of the field statistics of the archetypal PF wave event measured at polar cap latitudes in Earth's inner magnetosphere. In detail, the observed distributions $P(\log E)$ of wave fields are well fitted by prediction (3) of pure SGT, with reasonable

statistical significance. This is a strong argument that stochastic growth physics is relevant. The data are inconsistent with the uniform secular growth model familiar from the literature. SGT can thus explain the burstiness and widely varying wave fields, as well as the persistence of the waves and driving distribution over the observed range of altitudes. On the basis of the slightly better quantitative and statistical agreement of the observed $P(\log E)$ distributions with the prediction (4) of nonlinear SGT, weak evidence exists that a nonlinear process coexists with stochastic growth physics at high fields $\gtrsim 1$ mV m^{-1} and removes energy from the waves. Weak independent support for this nonlinear process comes from the existence and properties of a class of low frequency waves that appear to be correlated with the PF waves and may be the products of a nonlinear decay process for the PF waves. An analytic model is developed for why the PF waves reach an SGT state, involving propagation of an electron beam through MHD density irregularities and the development of fluctuations in the beam due to wave growth occurring in localized regions. For the polar cap plasma parameters considered, this model predicts that many beam fluctuations cross a growth site during the characteristic time for waves to grow (thereby justifying the use of the Central Limit Theorem for the wave statistics), that the beam fluctuations have timescales of several tens of milliseconds (well below most current detector capabilities), and that the wave burstiness should be of order that observed. The consistency of the PF wave statistics with SGT also implies the presence of local electron beams over much of the polar cap; the origin of this low-altitude source of electron beams is unknown.

Acknowledgments. The Australian Research Council and NASA grants NAG5-6369 and NAG5-6127 funded this work at the University of Sydney, while NASA GSFC grants NAG5-4497 and NAG5-7943 funded the research at the University of Iowa. We thank P. A. Robinson, S. P. Gary, and J. C. Dorelli for helpful discussions and comments on this paper.

Janet G. Luhmann thanks Paul J. Kellogg and another referee for their assistance in evaluating this paper.

References

Cairns, I. H., Detectability of electrostatic decay products in Ulysses and Galileo observations of type III solar radio sources, *Astrophys. J., 449*, L95, 1995.

Cairns, I. H., Measurement of the plasma density using the intensification of z mode waves at the electron plasma frequency, *Phys. Rev. Lett., 82*, 564, 1999.

Cairns, I. H., and J. D. Menietti, Radiation near $2f_p$ and intensified emissions near f_p in the dayside and nightside auroral region and polar cap, *J. Geophys. Res., 102*, 4787, 1997.

Cairns, I. H., and P. A. Robinson, First test of stochastic growth theory for Langmuir waves in Earth's foreshock, *Geophys. Res. Lett., 24*, 369, 1997.

Cairns, I. H., and P. A. Robinson, Constraints on nonlinear and stochastic growth theories for type III solar radio bursts from the corona to 1 AU, *Astrophys. J., 509*, 471, 1998.

Cairns, I. H., and P. A. Robinson, Strong evidence for stochastic growth of Langmuir-like waves in Earth's foreshock, *Phys. Rev. Lett., 82*, 3066, 1999.

Cairns, I. H., P. A. Robinson, and R. R. Anderson, Thermal and driven stochastic growth of Langmuir waves in the solar wind and Earth's foreshock, *Geophys. Res. Lett., 27*, 61, 2000.

Gary, S. P., and I. H. Cairns, Electron temperature anisotropy instabilities: Whistler, electrostatic and z mode, *J. Geophys. Res., 104*, 19,835, 1999.

Gary, S. P., Y. Kazimura, H. Li, and J.-I. Sakai, Simulations of electron/electron instabilities: Electromagnetic fluctuations, *Phys. Plasmas, 7*, 448, 2000.

Gurnett, D. A., The Earth as a radio source: The nonthermal continuum, *J. Geophys. Res., 80*, 2751, 1975.

Gurnett, D. A., S. D. Shawhan, and R. R. Shaw, Auroral hiss, z mode radiation, and auroral kilometric radiation in the polar magnetosphere, *J. Geophys. Res., 88*, 329, 1983.

Krall, N. A., and A. W. Trivelpiece, *Principles of Plasma Physics*, McGraw-Hill, New York, 1973.

LeDocq, M. J., D. A. Gurnett, and R. R. Anderson, Electron number density fluctuations near the magnetopause observed by the CRRES spacecraft, *J. Geophys. Res., 99*, 23,661, 1994.

Melrose, D. B., *Plasma Astrophysics*, vol. II, Gordon and Breach, Newark, N.J., 1980.

Melrose, D. B., *Instabilities in Space and Laboratory Plasmas*, Cambridge Univ. Press, New York, 1986.

Menietti, J. D., and J. L. Burch, "Electron conic" signatures observed in the nightside auroral zone and over the polar cap, *J. Geophys. Res., 90*, 5345, 1985.

Menietti, J. D., I. H. Cairns, C. W. Piker, and T. F. Averkamp, Statistical study of emissions near f_p and $2f_p$ in the dayside and nightside auroral region and polar cap, *J. Geophys. Res., 103*, 14,295, 1998.

Persoon, A. M., D. A. Gurnett, W. K. Peterson, J. H. Waite, Jr., J. L. Burch, and J. L. Green, Electron density depletions in the nightside auroral zone, *J. Geophys. Res., 88*, 1871, 1983.

Persoon, A. M., D. A. Gurnett, and S. D. Shawhan, Polar cap electron densities from DE 1 plasma wave observations, *J. Geophys. Res., 93*, 10,123, 1988.

Press, W. H., B. P. Flannery, S. A. Teukolsky, and W. T. Vetterling, *Numerical Recipes*, Cambridge Univ. Press, New York, 1986.

Robinson, P. A., Clumpy Langmuir waves in type III radio sources, *Sol. Phys., 139*, 147, 1992.

Robinson, P. A., Stochastic wave growth, *Phys. Plasmas, 2*, 1466, 1995.

Robinson, P. A., and A. Benz, Bidirectional type III solar radio bursts, *Sol. Phys., 194*, 345, 2000.

Robinson, P. A., and D. L. Newman, Two-component model of strong Langmuir turbulence: Scalings, spectra, and statistics of Langmuir waves, *Phys. Fluids B, 2*, 2999, 1990.

Robinson, P. A., I. H. Cairns, and D. A. Gurnett, Clumpy Langmuir waves in type III radio sources: Comparison of stochastic wave growth with observations, *Astrophys. J., 407*, 790, 1993a.

Robinson, P. A., A. J. Willes, and I. H. Cairns, Dynamics of Langmuir and ion-sound waves in type III radio sources, *Astrophys. J., 408*, 720, 1993b.

Shawhan, S. D., D. A. Gurnett, D. A. Odem, R. A. Helliwell, and C. G. Park, The plasma wave and quasi-static electric field instrument (PWI) for Dynamics Explorer-A, *Space Sci Instrum., 5*, 535, 1981.

Stix, T. H., *The Theory of Plasma Waves*, McGraw-Hill, New York, 1962.

Stix, T. H., *Waves in Plasmas*, Am. Inst. of Phys., College Park, Md., 1992.

Willes, A. J., and I. H. Cairns, Generalized Langmuir waves in magnetized kinetic plasmas, *Phys. Plasmas*, 7, 3167, 2000.

Zank, G. P., and I. H. Cairns, Pickup ion driven turbulence in the polar heliosphere: A stochastic growth model, *Astrophys. J.*, *541*, 489, 2000.

I. H. Cairns, School of Physics, University of Sydney, New South Wales 2006, Australia. (cairns@physics.usyd.edu.au)

J. D. Menietti, Department of Physics and Astronomy, University of Iowa, Iowa City, IA 52242, USA. (jdm@space.physics.uiowa.edu)

(Received November 13, 2000; revised May 21, 2001; accepted June 25, 2001.)